Studying Target Erosion in Planar Sputtering Magnetrons Using a Discrete Model for Energetic Electrons

C. Feist*[1], A. Plankensteiner[2], and J. Winkler[2]
[1]CENUMERICS, [2]PLANSEE SE
*Corresponding author: Haspingerstraße 16, A-6020 Innsbruck, Austria, Christian.Feist@cenumerics.com

Abstract: A discrete model for the prediction of relative ion bombardment flux and target erosion in planar sputtering magnetrons is implemented in COMSOL Multiphysics. Planar magnetrons are used within physical vapor deposition (PVD) processes to form thin film depositions on various types of substrates. The presented model portrays trajectories of energetic electrons within low pressure direct current (DC) gas discharges subjected to forces from the involved static electromagnetic fields and undergoing collisions with neutrals. Relative distributions of ion bombardment flux and target erosion are obtained by summation and projection of ionization collisions onto the target surface. An iterative scheme based on a series of consecutive transient analyses is adopted in order to guarantee convergence. The model is capable to resolve typical erosion profiles along with characteristic features such as the cross corner effect accurately. This is shown by application of the model to both an axisymmetric and a rectangular planar magnetron.

Keywords: sputtering, magnetron, target, erosion, plasma.

1. Introduction

Within planar sputtering magnetrons magnetically enhanced direct current (DC) gas discharges are used to form thin film depositions on various types of substrates [1]. Deposition material is eroded from a target through continuous bombardment by background gas ions (Fig. 1).

This way, ionization and erosion rates are increased allowing the process being operated at low pressure, which in turn increases deposition quality. As a drawback, however, varying magnetic field intensity in general leads to non-uniform erosion and low overall utilization of the target. This is seen by the characteristic erosion profiles of the targets and, furthermore, for rectangular planar targets by the so-called *cross corner effect* [2]. Thus, making target erosion more uniform together with increasing its utilization becomes an objective for process optimization.

In view of this, various attempts – both on the experimental and modeling field – have been made to understand and study the mechanisms taking place in magnetically enhanced DC discharges and to improve the design of magnetrons. The present work devoted to the development of an appropriate numerical model is motivated by efforts to improve lifetime of rectangular molybdenum (Mo) targets.

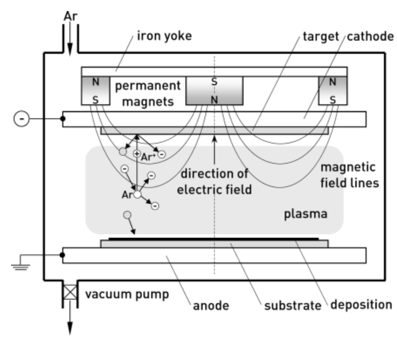

Figure 1. Schematic of planar DC sputtering magnetron [1] employing argon (Ar) as background gas.

2. Model and governing equations

The model presented in the following is based on a discrete approach in the spirit of the classical work of *Sheridan* and coworkers [3]. In the framework of such discrete models the gas discharge is described on a microscopic scale in terms of the involved species of charged particles such as electrons and ions. Charged particles are subjected to the *Lorentz* forces arising from the electromagnetic fields and to inter-particle collisions. Hence, discrete models – usually implemented by means of *Monte Carlo* codes – aim at tracing a statistically representative set of charged particles released in stochastic fashion and subjected to forces from reasonably assumed or *a priori* computed electromagnetic fields. Thus, weak coupling between the electromagnetic fields and the motion of charged particles and their spatial density is considered. Hence, these models are not able to provide a self-consistent solution such as kinetic or fluid-type descriptions do. Nonetheless, they are very attractive from a computational point of view since they do not require a spatial discretization of the computational domain (at least for computing the motion of charged particles).

2.1. Electromagnetic fields

Within a DC operated magnetron a static electric field **E** (*E-field*) and a static magnetic field **H** (usually termed as the *B-field* with respect to the magnetic flux density **B**) are present.

The electric field is established between the cathode subjected to a negative electric bias and the anode. To this end, the substrate or the reactor walls are usually grounded. For planar magnetrons it is reasonable to assume the electric field to be normal to the target or cathode surface $\mathbf{E} = E\,\hat{z} = -\mathrm{d}\Phi/\mathrm{dz}$ with z considered as the normal direction. The plasma can be considered neutral in an average sense with equal number density of electrons and ions $n_e = n_i \equiv n_0$ and separated from the cathode surface by a sheath. The potential Φ across the sheath can be described in analytical fashion such as by means of the improved *Child*'s law as proposed in [4]. The sheath is assumed to be connected to a pre-sheath within the plasma characterized by an almost constant electric field accelerating positively charged ions into the sheath. The potential drop across the pre-sheath is usually negligible as compared to the one across the sheath. The model is described in non-dimensional fashion [4] using the cathode bias Φ_w, the approximate plasma density n_0, and an estimate for the potential drop in the pre-sheath as its parameters.

The static magnetic field **H** and the corresponding magnetic flux density **B**, on the other hand, are generated by the presence of permanent magnets arranged on the backside of the cathode. The magnetic flux density **B** is a divergence-free field as described by *Gauss*'s law

$$\nabla \cdot \mathbf{B} = 0 \tag{1}$$

and related to the magnetic field **H** and remanent flux density $\mathbf{B}_R$ of the permanent magnets by a linear constitutive relationship using the permeability μ

$$\mathbf{B} = \mu \cdot \mathbf{H} + \mathbf{B}_\mathrm{R}. \tag{2}$$

The magnetic field can be solved for by means of the partial differential equation (PDE) formulated in terms of the scalar magnetic potential V_m

$$\mathbf{H} = -\nabla V_\mathrm{m}. \tag{3}$$

To this end, a finite element discretization can be adopted with prescribed values for the remanent flux density according to the employed permanent magnets. It should be noted that this way magnetic fields induced by the current through the discharge are neglected. This is, however, an acceptable simplification for process parameters commonly found in magnetrons.

2.2. Equation of motion of charged particles

A charged particle of mass m and charge q is subjected to the *Lorentz* forces from the electric field **E** and the magnetic flux density **B** expressed by the equation of motion

$$\mathbf{a} = \mathrm{q}/\mathrm{m} \cdot (\mathbf{E} + \mathbf{v} \times \mathbf{B}) \tag{4}$$

with $\mathbf{a} = \mathrm{d}^2\mathbf{x}/\mathrm{d}^2 t$ and $\mathbf{v} = \mathrm{d}\mathbf{x}/\mathrm{d}t$ as the particle acceleration and velocity vector, respectively. For given electric and magnetic fields the position vector $\mathbf{x}(t)$ of a charged particle can be solved for as a function of time t by means of numerical integration of the ordinary differential equation (ODE) (4). It is noteworthy that due to the magnetic term in (4) a charged particle experiences an out of plane force even for in-plane electromagnetic fields giving rise to the so-called *E* x *B drift motion*.

In a first step – neglecting collisions – equation (4) can be analyzed independently both for electrons ($q = -e$; $m = 1\, m_e$) and positive Ar^+ ions ($q = +e$; $m = 40\, u \approx 72{,}915\, m_e$) using appropriate initial conditions: Energetic electrons are released from the target surface as a consequence of ion bombardment and subsequent secondary electron emission (Fig. 1). With initial kinetic energies of a few eV, electrons are accelerated by the strong electric field through the sheath into the plasma allowing them to gain kinetic energies of a few 10^2 eV according to the electric bias applied to the cathode.

The strong magnetostatic field, on the other hand, provides confinement to the electrons within the plasma: for flux densities of a few 10^2 G electrons tyically exhibit gyro radii of a few millimeters and tend to swirl above the target (since their gyro radii are of the same order of magnitude as the characteristic length of the magnetic field their orbits, however, are not ideally helical). This way, electrons are able to ionize a series of Ar atoms ($e + Ar \rightarrow 2e + Ar^+$) until they are either lost from the confinement or almost all their kinetic energy is consumed and they contribute to the population of bulk electrons found in the plasma.

Consequently, Ar^+ ions, on the other hand, are primarily generated within the confinement zone established by the magnetic field. Due to their significantly larger mass they exhibit gyro radii of a few meters under the aforementioned magnetic field strengths. Thus, their response to the magnetic field is almost negligible at the length scale of industry size magnetrons and their trajectories almost do not deviate from the electric field lines. Hence, with the electric field assumed to act almost perpendicular onto the target, ions can be assumed to fall normally onto the target surface. Ion bombardment not only sputters deposition material atoms from the target but also provides the secondary electron emission flux required to maintain the process.

From the above it can be concluded that the in-plane positions of ions hitting the cathode and consequently the ones of sputtering and secondary electron emission can be determined from projecting the spatial positions of ionization events onto the target surface [3]. Hence, for modeling purposes this allows considering trajectories of electrons only without assessing the ones of the ions explicitly. In order to resolve the positions of ionization events in the model, collision events have to be triggered at random time instants for all electrons under consideration rather than modeling a "physical" collision between an electron and a neutral.

2.3. Collisions

Equation (4) describes the motion of charged particles without consideration of inter-particle collisions such as the ones occurring between electrons, between electrons and ions as well as between electrons and neutrals. Electron-ion collisions [3] and electron-electron collisions [5] usually can be neglected for weakly ionized plasmas such as can be found in magnetron discharges. Hence, only collisions between electrons and neutrals, i.e. Ar atoms, have to be accounted for. This not only allows resolving representative discrete positions of ionization events but also provides a mechanism for scattering of electrons out of the confinement after a certain time that otherwise would be indefinitely trapped within this region [3], which would be physically questionable.

Within the framework of the present model elastic, excitation, and ionization collisions are accounted for, whereas others such as superelastic scattering, two-step and penning ionizations are neglected [3]. Besides reducing the kinetic energy and velocity magnitude of the impinging electron the collisions lead to scattering of the electrons, i.e. to a change of the velocity direction vector. The energy loss depends on the type of collision: for ionization of ground state Ar it amounts to 15.8 eV plus the kinetic energy of the secondary released electron; for excitation it depends on the level of energy to which the Ar atom is excited (11.5 – 15.8 eV); for elastic scattering it is proportional to the mass ratio of the electron and the Ar atom.

According to classical collision theory collisions are characterized by differential cross-sections $d\sigma_c/d\Omega$ [1] (in units of area/steradian) serving as a measure for the probability of a given collision to take place and to scatter the impinging electron to a particular angle α. The differential cross-sections are different for each type of collision and depend on the kinetic energy of the impinging electron. Integration of the differential cross-section yields the integrated cross-section σ_c (in units of area) serving as a measure of probability for a particular collision to take place. From summation of the integrated cross-sections $\sigma_{c,i}$ over all $i = 1, \ldots, p$ types of collisions the total collision cross-section σ along with the corresponding collision frequency [1] is obtained.

3. Implementation in COMSOL Multiphysics

The model given in Section 2 has been implemented in COMSOL Multiphysics 4.3a (the current version at the time of implementation) for both 2D axisymmetric and 3D settings.

3.1. Electromagnetic fields

To this end, the electric field component normal to the target surface described by the improved *Child*'s law [4] (see also Section 2.1) is modeled using a set of fully parameterized analytical functions.

The magnetic field **H** (3) and magnetic flux density **B** (2) are computed using the *Magnetic Fields, No Currents (mfnc)* interface with the remanent flux density of the permanent magnets assigned to the corresponding constitutive relationship (2). The magnetic fields are solved for on an appropriate 2D or 3D geometric representation of the permanent magnets, the ferromagnetic yoke, and the target/cathode assembly. Since most of the other components of the reactor are usually made of materials of low relative magnetic permeability ($\mu \approx 1$), the entire surrounding can be considered as vacuum and modeled as a primitive such as a sphere or cylinder.

Due to the assumption of weak, i.e. non self-consistent coupling the magnetic fields are computed *a priori* using a stationary study step. There are no particular requirements with respect to the finite element discretization as long as a sufficiently fine resolution of the magnetic flux density within the expected confinement zone is provided. Thus, together with solving for a scalar field (3) only, computational costs are low even for 3D models of industry-scale magnetrons with targets of 1 to 2 m in length.

3.2. Trajectories of energetic electrons

With the electromagnetic fields at hand the equation of motion (4) is implemented for energetic electrons using the *Point ODEs (pode)* interface. The latter is assigned to an arbitrary large set of m_e points corresponding to the desired representative number of electrons. In order to account for electron release from the target through secondary electron emission, initial values for the positions $\mathbf{x}(t = 0)$ on the target are assigned to these points in random fashion. To this end, a random function for each point and a probability density function for electron emission on the target surface are defined. Since the flux of electrons emitted from the target is proportional to the flux of ions bombarding the target, the electron emission density function can be continuously updated according to the positions of ionizations taking place over time integration of the ODE (4). Thus, the electron emission probability density function also provides a measure for convergence. At the beginning of the analysis, the density function has to be initialized (either as a simple uniform distribution or based on experience). Clearly, convergence is obtained faster if the initial density function already resembles the expected distribution.

The electrons' initial velocities can be derived from the work function [1] of the target material, even though these are of no significant importance since initial kinetic energies are usually small as compared to the energies gained by the electric field.

Collisions are considered as discontinuities of the velocity vector **v** of individual electrons and are triggered in random fashion. To this end, random numbers – sampled for all electrons under consideration – are compared to the probability per time step for a collision to occur. The latter is continuously computed from the total cross-section of the electron based on its kinetic energy. If a collision is found to take place, the collision type is determined using another random number compared to the relative probability of each collision type. The colliding electron's velocity vector **v** in equation (4) is then reinitialized according to the energy loss corresponding to the particular type of collision and scattering angle α. The latter is determined from a third random number that is compared to the relative probability for a particular angle based on the differential cross-section $\mathrm{d}\sigma_c/\mathrm{d}\Omega$. These are taken as the ones for elastic scattering [6] and are assumed to be approximately valid in a relative sense for all three types of collisions under consideration [3].

In this context, the *Events (ev)* interface has been successfully employed. An *Implicit Event* feature is used to trigger a collision. Particle velocity vectors are then reinitialized using a *Reinitialization on Points* sub-feature. *Indicator States* are used as global counters for the various collision events.

Finally, a *Boundary ODEs and DAEs (bode)* interface is employed on the target surface in order to compute the relative ion bombardment flux by means of a histogram for collision counting. The latter is implemented as a dummy interface only, with collision counting done by the *Reinitialization on Boundary* sub-feature of the implicit events feature described above. After normalization the relative ion bombardment flux is used as an update for the electron emission density function.

Equations of motion (4) together with all auxiliary equations are integrated over time using a BDF scheme. Integration is carried out until only a small percentage (e.g. 5%) of the electrons is still able to perform ionizations (i.e. $\varepsilon \geq 15.8$ eV), which usually takes place after a few µs. To this end, a stop condition is used within the corresponding time dependent study step. Time step size (typically 10 to 50 ps) is chosen in order to appropriately resolve typical gyro radii and the sheath thickness. During time-integration a general extrusion operator is used to obtain the values of the magnetic flux density **B** taken from the preceding stationary study step at the electron's position $\mathbf{x}(t)$. Electric field values are directly computed using the set of parameterized functions.

The time dependent study step is contained within a parametric sweep feature over m_{run} in order to conduct a series of consecutive runs. This way, the electron emission density function can be updated until convergence is obtained.

3.3. Final remarks on the implementation

The present implementation uses the *Point ODEs (pode)* interface for computing the electrons's trajectories instead of the ready-made *Charged Particle Tracing (cpt)* interface for various reasons: Firstly, the *Elastic Collision Force* feature – accounting for *Monte Carlo* type collision models – implemented in the current version 4.3b was not available at the time of development of the present model. Secondly, the *Events (ev)* interface cannot be used together with the particle tracing interface. Finally, collision statistics (i.e. counting of discrete events) are not feasible together with the particle tracing interfaces. Even with the current version 4.3b this cannot be achieved such that the presented model is still fully relevant.

As a drawback, however, COMSOL's attractive visualization features for particle tracing are not available for the present implementation. Thus, only simple 2D projections of the trajectories without solution-based coloring can be produced.

DC discharges could also be described by means of self-consistent fluid-type models such as available within COMSOL's Plasma Module. With the respective constitutive properties becoming anisotropic due to the presence of a strong magnetic field, magnetrons, however, are difficult to model. Furthermore, they require a considerably fine spatial discretization resulting in significant computational costs.

4. Examples

Within the following, two representative application examples will be given, for both 2D axisymmetric and 3D problems. The examples are taken from literature and served for verification purposes during model-development.

4.1. Axisymmetric planar magnetron

The first example is taken from the publications of *Sheridan* and coworkers [3, 7] and deals with an axisymmetric planar magnetron. The latter consists of a copper cathode of app. 108 mm in diameter also serving as a target and placed above an array of permanent magnets coaxially arranged around a central cylindrical magnet. Magnetic short-circuit is established by an iron yoke. Argon (Ar) is used as background gas. The unknown characteristics of the magnets are calibrated by the values given in [7]. Maximum flux density magnitude on target level is app. 600 G at the magnetron axis. At $r \approx 19$ mm the magnetic field becomes parallel to the target with $|\mathbf{B}| \approx 240$ G. This is empirically known to be the location of maximum target erosion [2].

A cathode bias of $\Phi_{\text{w}} = -400$ V and a plasma density of $n_0 = 2\ 10^{10}$ cm^{-3} resulting in a sheath thickness of app. 3 mm are assumed. Neutral number density is estimated from the ideal gas law with $p = 1$ Pa (7.5 mTorr) and $T = 20$°C yielding an ionization degree of app. $\beta \approx 8\ 10^{-5}$.

Magnetic fields are computed using a 2D axisymmetric representation using an effective remanent flux density for the outer magnets accounting for the solid fraction resulting from the array-type arrangement.

Exemplary orbits of ten electrons (for the sake of clarity sampled from the considered set of electrons) are shown in Fig. 2 projected onto the rz-plane (top) and $r\varphi$-plane (bottom). Orbits are given over an initial period of 0.1 µs for the first three runs $m_{\text{run}} = 1\ldots3$ (from left to right). For the first run (left) uniform probability density for secondary electron emission over the radial coordinate of the cathode surface is assumed, whereas an updated function is used for the consecutive runs. Initial positions of electrons are indicated by square symbols, whereas the current positions (or the positions of rest of inactive electrons) are given by circles. It is clearly seen that electron emission density rapidly converges reducing the probability for emission of unconfined electrons: Within the first run (left) 50% of the electrons have left the computational domain after just 0.1 μs because of being unconfined by the electromagnetic fields, whereas within the third run (right) all electrons are still active. Nonetheless, they will be scattered out of the confinement due to collisions during further runtime, thus, gradually reducing the number of active electrons. Some kinks in electron trajectories (best seen by their $r\varphi$-plane projections in Fig. 2) indicate first collision events accompanied by obvious scattering. For the seventh run (not shown) app. 30% of the electrons are still active after a period of 2.5 μs. However, only about 7% of the initial electron population is capable to perform ionizations.

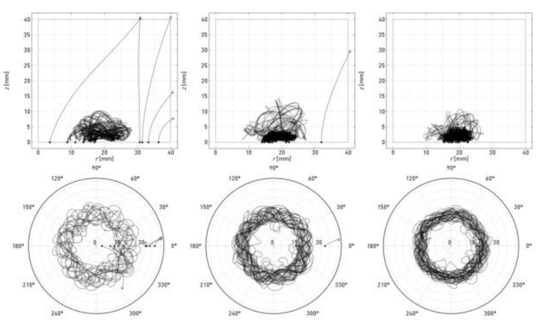

Figure 2. Electron orbits for ten randomly selected electrons over an initial period of 0.1 μs for the first three runs (from left to right) in *rz*-plane (top) and $r\varphi$-plane (bottom) with initial and current positions (or positions of rest of inactive electrons) indicated by square and circle symbols, respectively.

Fig. 3(a) depicts the cumulative number of ionization events in the *rz*-plane normalized using the maximum value as obtained after seven runs. The maximum ionization density is found in the interval $r = [19, 20]$ mm. After integration of the cumulative number of ionization events along the *z*-axis one obtains the relative radial ionization profile which can be considered to be proportional to target erosion rate. In view of this, Fig. 3(b) shows the obtained erosion profile normalized by the target thickness of 4.76 mm. It can be seen that maximum ionization density and target erosion take place at $r \approx 19$ mm which perfectly correlates to the empirical observation mentioned above.

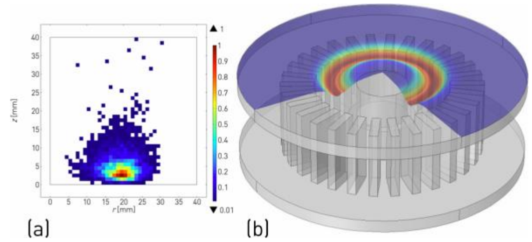

Figure 3. (a) Normalized ionization density in *rz*-plane and (b) predicted relative target erosion normalized by target thickness.

4.2. Rectangular magnetron

Finally, application of the developed model to a fully 3D setting is shown by means of the generic rectangular magnetron investigated by *Fan* and coworkers [2] in view of the so-called *cross corner effect*. The magnetron under consideration and shown in Fig. 4 consists of a rectangular target of 520 mm x 120 mm in size and 12 mm thickness. The target is placed above a central line magnet and a closed outer ring magnet connected by a ferromagnetic pole-plate. The considered configuration for the permanent magnets is typical for industrial planar magnetrons used within arrays for forming thin-film depositions on large planar components as architectural glasses or similar. The polarity of the magnets determines the drift direction for electrons along the racetrack between the magnets (Fig. 4(b)).

In view of the two-fold symmetry the magnetostatic problem can be analyzed on a quarter-segment of the entire assembly. Electron trajectories are, however, integrated considering the entire domain. There would be no particular advantage in considering any (anti)symmetry due to the lack of need for spatial discretization. Integration of the ionization density and computation of the normalized erosion are, however, performed making use of antisymmetry (attention must be paid when setting up the required extrusion coupling operators due to different symmetry conditions). This is also indicated by the erosion distribution normalized by target thickness, which already exhibits the characteristic racetrack as shown in Fig. 4(a). However, by taking a closer look to the erosion distribution in top view (Fig. 4(b)) it can be seen that the erosion profile is not homogeneous along the electrons' drift direction. Instead, predicted maximum target erosion occurs where electrons leave the curved end sections and enter the straight portions. These results are fully consistent with the findings given in [2]. Since this anomaly takes place at both curved end sections and due to antisymmetry it is observed at opposite or “cross corners”. Hence, two regions of fairly small size become the limiting factor for target utilization (targets cannot be sputtered when becoming perforated due to the danger of damaging the cathode and spurious depositions of cathode material). For the present case using an integration operator it was computed as app. 18%.

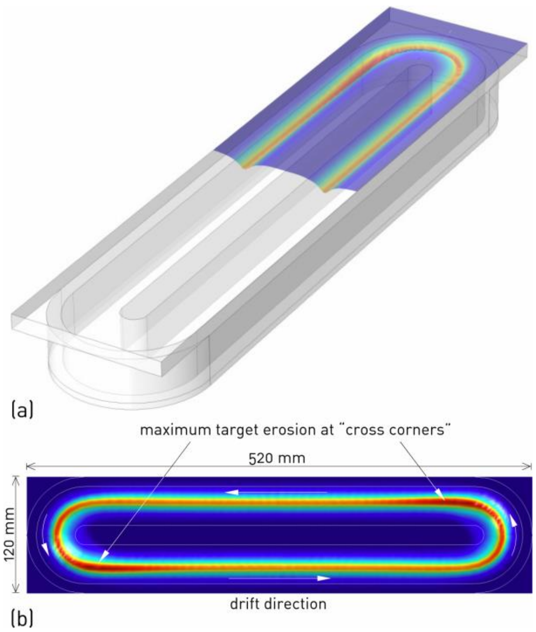

Figure 4. (a) Geometric representation and (b) top view of rectangular sputtering magnetron with predicted normalized erosion profile.

5. Summary and outlook

Application of the presented discrete model for energetic electrons in planar sputtering magnetrons to an axisymmetric planar and a rectangular planar magnetron demonstrates its fidelity and soundness. The obtained results perfectly agree to experimental findings as documented in the literature and from in-house experience. This is at least true in a relative sense in terms of normalized erosion distributions and the resolution of characteristic features such as the cross corner effect. A quantitative prediction of erosion rate and life-time cannot be obtained from the model. This, however, was out of scope for the present modeling efforts.

Even though discrete models of *Monte Carlo* type can be considered as a classical means in analysis of plasma-physics, the present model unifies all involved computations within in a single computational framework by using COMSOL Multiphysics. Such models usually rely on a combination of tools with the need for interfacing and data-exchange between the latter.

For future work the model will be employed to study design modifications on both magnetrons and targets in order to render target erosion profiles more uniform and to increase overall target utilization.

6. References

1. M.A. Lieberman and A.J. Lichtenberg, *Principles of Plasma Discharges and Materials Processing*, Second Edition, John Wiley & Sons Inc., Hoboken (NJ) (2005)
2. Q.H. Fan, L.Q. Zhou, and J.J. Gracio, A Cross-Corner Effect in a Rectangular Sputtering Magnetron, *J. Phys. D: Appl. Phys.*, **36**, 244-251 (2003)
3. T.E. Sheridan, M.J. Goeckner and J. Goree, Model of Energetic Electron Transport in Magnetron Discharges, *J. Vac. Sci. Technol. A*, **8**(1), 30-37 (1990)
4. T.E. Sheridan and J. Goree, Analytic Expression for the Energetic Potential in the Plasma Sheath, *IEEE Trans. Plasma Sci.*, **17**(6), 884-888 (1989)
5. S.M. Rossnagel, J.J. Cuomo, and W.D. Westwood (eds.), *Handbook of Plasma Processing Technology – Fundamentals, Etching, Deposition, and Surface Interactions*, Noyes Publications, Park Ridge (NJ) (1990)
6. S.N. Nahar and J.M. Wadehra, Elastic Scattering of Positrons and Electrons by Argon, *Phys. Rev. A*, **35**(5), 2051-2064 (1987)
7. T.E. Sheridan and J. Goree, Low-Frequency Turbulent Transport in Magnetron Plasmas, *J. Vac. Sci. Technol. A*, **7**(3), 1014-1018 (1989)